Omnidirectional Dual-reflector Antenna with a GO Shaped Main Reflector for an Arbitrary Far-field Pattern in the Elevation Plane

S. R. Zang[#1], J. R. Bergmann[#1], and F. J. S. Moreira[*2]

[#]*PUC-Rio, CETUC*
Rua Marques de São Vicente 225, 22453-900, Rio de Janeiro, Brazil
[1]sandro@cetuc.puc-rio.br, bergmann@cetuc.puc-rio.br

[*]*UFMG*
Av. Antônio Carlos 6627, 31270-901, Belo Horizonte, MG, Brazil
[2]fernandomoreira@ufmg.br

***Abstract* - This work presents a formulation for shaping the main reflector of a dual reflector antenna designed to offer an omnidirectional coverage with an arbitrary radiation pattern in the vertical plane. The subreflector is generated by an axis-displaced ellipse and the main reflector is shaped to achieve a prescribed far-field radiation pattern. The shaping procedure is based on geometrical optics (GO) principles. The GO shaping results are validated by analysis provided by the accurate method of moments technique.**

I. INTRODUCTION

The growing interest on high-speed Internet access for residential and small business costumers has created a demand for last-mile broadband access. In this scenario, wireless technologies show lower costs, rapid deployment, and lower maintenance. Wireless links at millimeter waves make attractive the use of compact reflector antennas, capable of providing wider absolute bandwidths necessary to transmit wideband signals. Single and dual reflector antennas have been investigated for omnidirectional coverage [1,2]. The reflector surfaces are bodies of revolution obtained by spinning confocal conic sections or shaped generating curves about a symmetry axis (Fig. 1).

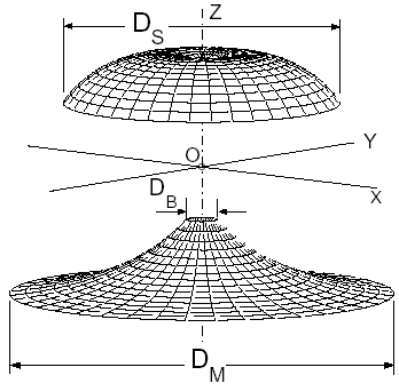

Figure 1 - Circular symmetric reflector surfaces.

As demonstrated in [2], the dual-reflector antenna leads to more compact designs than the single reflector concept, as the dual configuration requires considerably smaller reflector diameter to achieve the necessary aperture width for adequate control of the radiation pattern in the elevation plane. Besides compactness, axis-displaced dual-reflector configurations offer the additional advantage of controlling the feed return loss by minimizing the subreflector radiation toward the feed horn [2]. Furthermore, the antenna main beam can be pointed below horizon to reduce interference in LMDS scenarios [2].

In this work, we present a simple and efficient shaping procedure for omnidirectional dual-reflector antennas based on geometrical optics (GO) principles. To control the antenna radiation pattern in the elevation plane, the proposed configurations have a GO shaped main reflector, which may have real or virtual caustic, yielding different options for the antenna designer. To minimize the feed return loss, the subreflector can be generated by an axis-displaced ellipse (ADE), as suggested in [2]. The design procedure is exemplified by a design exploring the potentialities of these omnidirectional dual-reflector configurations as base-station antennas in point-multipoint radio links with tilted main beams. To ensure vertical polarization, the dual-reflector antenna designs are fed by the coaxial TEM horn as illustrated in Figure 2.

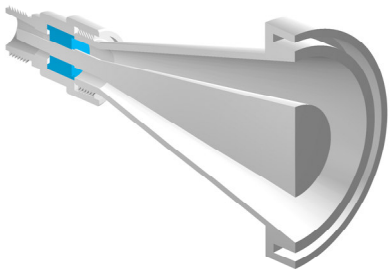

Figure 2 – TEM coaxial horn

In order to estimate electrical performance of the proposed design procedure, a full-wave stepped-waveguide model and MoM/HFIE method are combined to analyse both the fields in the interior region and the exterior current contributions of the feed horn [3]. The interaction is accurately analysed by using the EFIE on the exterior surfaces of the coaxial horn. The

equivalence currents principle is introduced to formulate the HFIE on the radiating aperture which combines the interior field transition problem with the exterior radiation. Due to the TEM mode excitation, only the TEM and TM modes are considered at the transition. The application of the analysis technique yields the antenna radiation pattern as well as the antenna return loss at the end of the N-type connector.

II. ANTENNA ANALYSIS

The analysis is subdivided in two parts, starting from the analysis of the transition between the feeding waveguide and the coaxial horn aperture. The horn is represented as series of stepped coaxial waveguides sections and Mode Matching is performed by rigorously enforcing the boundary conditions at each step. It results a scattering matrix [S] for the entire transition region:

$$\begin{bmatrix} b^C \\ b^A \end{bmatrix} = \begin{bmatrix} S_{11} & S_{12} \\ S_{21} & S_{22} \end{bmatrix} \begin{bmatrix} a^C \\ a^A \end{bmatrix} \tag{1}$$

which relates incident and reflected modes at the two extremes of the transition region. In (1), the vectors $[a^C]$ and $[a^A]$ contain the amplitudes of incident modes at the region ´C´ and ´A´, respectively, whereas the vectors $[b^C]$ and $[b^A]$ contain the amplitudes of reflected modes at the connector ´C´ and aperture´A´, respectively (see Figure 3). Considering the TEM fundamental mode as the only incident mode at region C and the circularly symmetric structure, only the TEM and TM are excited throughout the entire transition region, as the TE mode do not couple with the TEM excitation. The matrix [S] depends on the geometrical parameters and on the wavelength as well as the number of modes considered to ensure continuity of the electric and magnetic throughout the transition region. Part of the power of the modes reaching the aperture, region A, is radiated into the space while the rest is guided back into the horn.

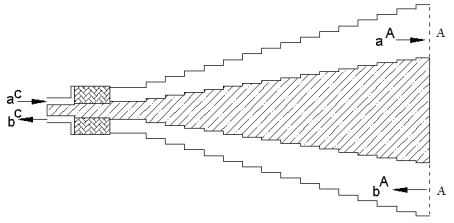

Figure 3 - Horn represented as series of stepped coaxial waveguides sections

In the second part of the analysis scheme, to calculate the radiate fields and the amplitude of the reflected modes $[b^A]$, the MoM is employed to solve the EFIE and MFIE, as described in [3]. To apply the above strategy, an equivalent to the actual electromagnetic problem is defined by replacing the feed radiating aperture by a sheet of perfect conductor with an equivalent magnetic current density

$$\vec{M}\left(\left[a^A\right],\left[b^A\right]\right) = -\sum_{l=1}^{N_M}\left(a_l^A + b_l^A\right)\left(\hat{n}\times\hat{e}_l^A\right) \tag{2}$$

where $\hat{n}$ is the unit vector normal to the aperture, $\hat{e}_l^A$ is the electric field of the modes internal to the aperture. The magnetic current density $\vec{M}$ radiates into the space and induces an electric surface current $\vec{J}$ on the metallic wall of the equivalent problem. These currents ensure the continuity of the tangential magnetic field across the aperture and zero tangential electric field on the metallic surface at the aperture and reflectors:

$$\begin{aligned} \vec{n}\times\left[\vec{E}^S(\vec{J}) + \vec{E}^S(\vec{M})\right] &= 0 \\ \vec{n}\times\left[\vec{H}^S(\vec{J}) + \vec{H}^S(\vec{M})\right] &= \hat{n}\times\vec{H}^A \end{aligned} \tag{3}$$

where $\vec{E}^S$ and $\vec{H}^S$ are electromagnetic field scattered by the currents $\vec{M}$ and $\vec{J}$.

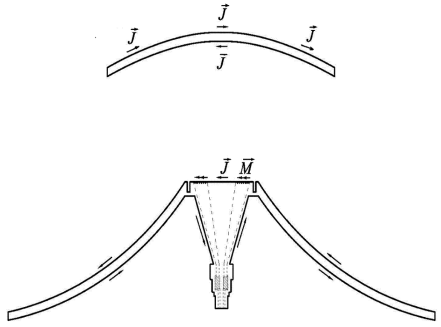

Figure 4 - HFIE model of the outside surface currents of the feed main reflector

To apply the MoM solution, the current densities $\vec{M}$ and $\vec{J}$ are expanded by sub sectional roof-top patch modes $\vec{P}_j^J$ and $\vec{P}_k^M$ respectively. In this way, a conversion matrix [**V**] is introduced to transform the roof-top patch modes into eigenmodes of the aperture fields:

$$\begin{aligned} \vec{J} &= \sum_{j=1}^{N_S} \bar{J}_j \vec{P}_j^J \\ \vec{M} &= \sum_{l=1}^{N_M} \vec{M}_l \sum_{k=1}^{N_A} V_{lk} \vec{P}_k^M \end{aligned} \tag{4}$$

where N_S and N_A are the number of roof-top patch modes on the entire surface and on the aperture, respectively, and N_M is the number of modes TEM and TM used to approximate the aperture fields. By testing the EFIE with $\vec{P}_i^J$, it leads to the following matrix equation:

$$[J] = \frac{1}{\eta}[Z]^{-1}[Q][V]^T[M] \tag{5}$$

where the vector [M] is obtained from the amplitude (a_l^A and b_l^A) of the aperture field modes and the elements of the matrices [Z] and [Q] are given by

$$Z_{ij} = -\frac{1}{\eta}\int_{S_i}\int_{S_j} \vec{P}_i^J \cdot \vec{E}^S(\vec{P}_j^J)\,ds_i ds_j$$

$$Q_{ik} = \int_{S_i}\int_{S_k} \vec{P}_i^J \cdot \vec{E}^S(\vec{P}_k^M)\,ds_i ds_k \tag{6}$$

On the other hand, testing the MFIE with $\hat{n}\times\vec{e}_l^A$ and combining with the relation of (1), it is possible to define a relation between the vectors [a^C] and [b^C] that leads to the following matrix equation:

$$\left[b^C\right] = \left\{[S_{11}] + [S_{12}]\left(\left[S_{11}^A\right] - [S_{22}]\right)^{-1}[S_{21}]\right\}\left[a^C\right] \tag{7}$$

where

$$\left[S_{11}^A\right] = \left(\left[Y^{INT}\right] + \left[Y^A\right]\right)^{-1}\left(\left[Y^{INT}\right] - \left[Y^A\right]\right) \tag{8}$$

$$\left[Y^A\right] = [V][Q][Z]^{-1}[Q][V]^T + [V]\left[Z^A\right][V]^T \tag{9}$$

$$\left[Y^{INT}\right] = \left[\left\langle \hat{n}\times\vec{e}_l^A, \hat{n}\times\vec{H}^A\right\rangle\right] \tag{10}$$

and [Z^A] is a subset of [Z] for the modes on the aperture.

III. OMNIDIRECTIONAL SHAPED DUAL REFLECTOR

Figure 5 illustrates the omni directions axis-displaced antenna (OADE). The antenna is composed of two circularly symmetric reflectors with a common symmetry axis. The subreflector is generated by an axis-displaced ellipse and the foci of the generating ellipse are at the origin O of the coordinate system and at point *P*. After the rotation around the z-axis, *P* generates an annular caustic.

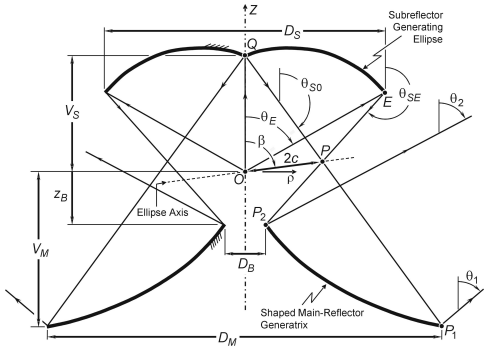

Figure 5 - Dual reflector generatrices of the shaped OADE antenna.

The OADE antenna is illuminated by a feed point source at *O* with circularly symmetric radiation pattern $G_F(\theta_F)$, where θ_F is the angle of the feed ray with the *z*-axis. After two reflections, the spherical wavefront emanating from *O* will be transformed into a spherical wavefront at the far-field region with a corresponding omnidiretional radiation pattern $G_A(\theta)$, where θ is the angle of observation with the *z*-axis.

By applying GO principles, the main-reflector generatrix will be shaped to reflect the rays coming from the annular caustic *P* toward the far-field region to obtain a specified radiation pattern in the elevation plane. The GO transformation $G_F(\theta_F) \rightarrow G_A(\theta)$ can be obtained by two different ray structures emerging from the main reflector and directed toward the far-field region. They differ from each other in the location of the main-reflector caustic, which can be virtual or real. Consequently, they yield main-reflector with different shapes and dimensions. For the shaping, we have adopted a procedure based on [5], which was originally proposed for the GO shaping of offset single reflectors. Following [5], the main reflector is represented by a real function $L(\eta_S)$, such that a point at this surface is located by the position vector

$$\vec{r}_M(\theta_S) = \left[\rho_P + 2\eta_S e^{L(\eta_S)}\right]\hat{\rho} + \left[z_P + \left(\eta_S^2 - 1\right)e^{L(\eta_S)}\right]\hat{z}, \tag{11}$$

where ρ_P and z_P are the cylindrical coordinates of *P* and $\eta_S = \cot(\theta_S/2)$. From the law of reflection, the relation between the incident and reflected ray directions at the main-reflector surface is given by [5]:

$$\frac{dL(\eta_S)}{d\eta_S} = \frac{2}{\eta - \eta_S}, \tag{12}$$

where $\eta = \cot(\theta/2)$. The numerical integration of (12) gives the values of $L(\eta_S)$, when replaced in (11) yields the reflector surface. The integration of (12) can be performed in terms of θ_F, by varying it from 0 to θ_E.

To conclude the GO shaping procedure one should establish the relation between the far-field direction θ and θ_F, which can be obtained by imposing the law of energy conservation to the bundle of rays departing from *O* and leaving the main reflector after both reflections:

$$\int_0^{\theta_F} G_F(\theta_F')\sin\theta_F'\,d\theta_F' = N\int_{\theta_1}^{\theta} G_A(\theta')\sin\theta'\,d\theta', \tag{13}$$

where *N* is a normalization factor. The limits of the farfeld radiation pattern are given *by* $\theta = \theta_1$ and θ_2 and they are associated to $\theta_F = 0$ and θ_E, respectively.

The numerical evaluation of (12) determines $L(\eta_S)$ to within a constant of scale, i.e., an infinite set of main reflectors, differing from each other by a scale factor, provide the same far-field pattern $G_A(\theta)$, under a GO perspective. To uniquely determine the main reflector, the present shaping procedure assumes a fixed location for P_2 given by the input parameters D_B and z_B (see Fig. 5). Finally, for the case studies discussed in the next section a fourth-order Runge-Kutta method was employed to numerically integrate (12).

IV. CASE STUDIES

To illustrate the design procedure described in the previous section and to explore the potentialities of OADE as base-station antenna in point-multipoint radio links, the main reflector is shaped to generate a radiation pattern with a cosecant square pattern $G_A(\theta)$ in the elevation plane, that provides a uniform coverage of ground around the antenna.

For GO main-reflector shaping, the feed radiation pattern was represented by

$$G_F(\theta_F) = G_{FO}[[J_0(kr_i \sin\theta_F) - J_0(kr_e \sin\theta_F)]]/[\sin\theta_F]]^2 , \quad (12)$$

where G_{FO} is a normalization factor. It represents the radiation from a coaxial aperture mounted on a perfect electric conductor plane, with internal and external radii r_i and r_e, respectively. In the present case study, $r_i = 0.45\lambda$ and $r_e = 0.9\lambda$. As the horn aperture dimensions are electrically small, the feed phase center is practically at the horn's aperture plane.

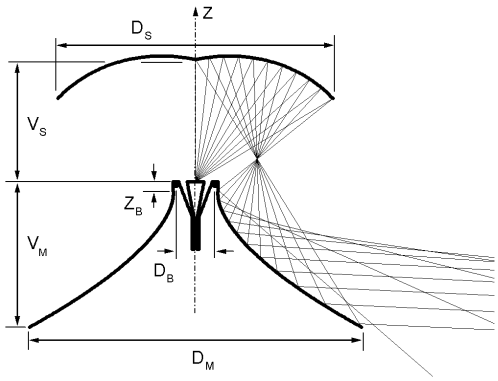

Figure 6 - shaped generating curves about a symmetry axis

For comparison purposes, the classical OADE configuration described in [2] is used as reference. In [2] the antennas were designed to provide a main beam tilted 12° away from the horizon with input parameters $z_B = 0$ and $D_B = 2.4\lambda$, providing enough space to accommodate the horn's structure. The subreflector parameters $D_S = 14.71\lambda$ and $V_S = 7.636\lambda$ were established to attain the desired main-beam tilt $\theta = 102°$ (i.e., 12° below horizon) together with a subreflector edge angle $\theta_E = 55°$. The values of the main-reflector projected diameter $D_M = 17.56\lambda$ and of the conical aperture width $W_A = 7\lambda$ were also specified, according to the design procedure for classical configurations [2]. Such aperture width W_A provided half-power beam widths with approximately 10°.

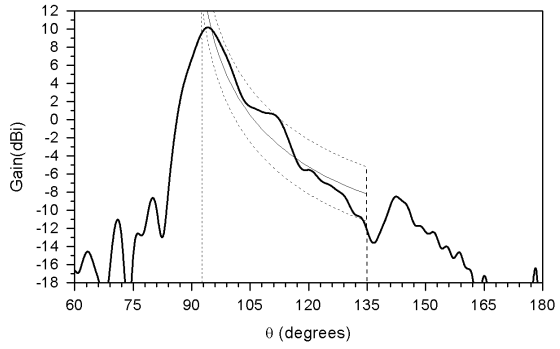

Figure 7- Antenna radiation pattern on the vertical plane

By using the subreflector described before, the main reflector was shaped to produce the cosecant squared radiation pattern between $\theta_1 = 93°$ and $\theta_2 = 135°$ and with a real main reflector caustic, as illustrated in Fig. 6. The full-wave analysis described in Sect. II was conducted to validate the shaping procedure and the antenna radiation pattern is illustrated in Fig. 7, where the dashed line is the desired cosecant squared radiation pattern between $\theta = 93°$ and 135° and its ±3 dB limits.

Figure 8 shows the antenna return loss obtained by employing a conical coaxial horn (dashed line) with a maximum of −15.7dB along the frequency band. As observed in [4], the largest contribution to the return loss comes from the small size aperture horn usually required for the designs. The MoM/HFIE method can be combined with an optimization algorithm to shape the coaxial horn to reduce the antenna return as illustrated by the full line in Fig. 8. It shows a peak of −18.dB along the band. In both cases the coaxial horn has the same aperture size in order to control the feed radiation pattern.

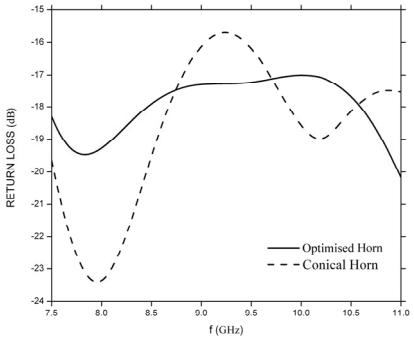

Figure 8 – Antenna return loss

V. CONCLUSIONS

A GO-based formulation for shaping the main reflector of dual-reflector omnidirectional antennas with arbitrary radiation pattern in the vertical plane was presented. To illustrate the design procedure, an OADE configuration was synthesized to generate a radiation pattern with a cosecant square pattern, providing uniform coverage. A full-wave analysis was conducted to validate the shaping procedure.

REFERENCES

[1] A. P. Norris and W. D. Waddoup, "A millimetric wave omnidirectional antenna with prescribed elevation shaping," in Proc. ICAP—4th Int. Conf. Antennas and Propagation, 1985, pp. 141–145.

[2] F. J. S. Moreira and J. R. Bergmann, "Axis-Displaced Dual-Reflector Antennas for Omnidirectional Coverage with Arbitrary Main-Beam Direction in the Elevation Plane", IEEE Trans. Antennas Propagat., vol. 54, no. 10, pp. 2854–2861, Oct. 2006.

[3] Kefeng Lui, C. Balanis, C. Birtcher, and G. Barber, "Analysis of Pyramidal Horn Antennas Using Moment Methods", IEEE Trans. Antennas Propagat., vol. 41, no. 10, pp. 1379–1389, Oct. 1993.

[4] J. R. Bergmann and F. J. S. Moreira, "An omni directional ADE reflector antenna," Microwave Opt. Tech. Lett., vol. 40, 3, pp. 250–254, Feb. 5, 2004.

[5] Westcott, B. S., Stevens, F. A., and Brickell, F.: 'GO synthesis of offset dual reflectors', IEE Proc., 1981, 128, Pt. H, (1), pp.11–18